processes

MDPI

Article

A Mathematical Modeling of the Reverse Osmosis Concentration Process of a Glucose Solution

Chenghan Chen * and Han Qin

Biomass Energy Technology Research Center, Biogas Institute of Ministry of Agriculture, Chengdu 610041, China; qinhan@caas.cn

* Correspondence: chenchenghan@caas.cn

Received: 21 March 2019; Accepted: 27 April 2019; Published: 8 May 2019

Abstract: A mathematical modeling of glucose–water separation through a reverse osmosis (RO) membrane was developed to research the membrane's performance during the mass transfer process. The model was developed by coupling the concentration–polarization (CP) model, which uses one-dimensional flow assumption, with the irreversible thermodynamic Spiegler–Kedem model. A nonlinear parameter estimation technique was used to determine the model parameters L_p (hydraulic permeability constant), σ (reflection coefficient), and B_s (solute transport coefficient). Experimental data were obtained from the treatment of a pre-treated glucose solution using a laboratory-scale RO system, and studies on the validation of the model using experimental results are presented. The calculated results are consistent with the experimental data. The proposed model describes the RO membrane concentration process and deduces the expression of k (mass transfer coefficient in the CP layer). The verification shows that the expression of k well-describes the reverse osmosis mass transfer of a glucose solution.

Keywords: reverse osmosis; mass transfer process; concentration polarization; mathematical model

1. Introduction

In the last few decades, in China, with the development of industry and the increase in pollution, water shortage has been getting worse. Wastewater recycling can effectively alleviate this situation and contribute to the sustainability of development. Considering the relatively efficient and simple process, membrane technology is a promising method for water treatment [1–4]. Additionally, it is reported that reverse osmosis (RO) technology is a relatively appropriate technique for manipulating sugar concentration [5]. In recent years, RO has gained widespread interest and has become a widely adopted modern tool for industrial applications and research laboratories. This has resulted in a great demand for RO membranes, making it necessary to reduce the cost of the RO system. According to the literature reported [6], the development of a proper mathematical model that adequately describes the performance of the RO process is crucial for the optimum design of an RO membrane which can make the RO system more efficient, thereby reducing the overall cost.

A number of mechanistic and mathematical models have been proposed to describe the mass transfer and hydrodynamic permeability in RO. In the RO separation processes, the mass transfer is mainly governed by the inside-membrane mass transfer and the outside-membrane mass transfer. The inside-membrane mass transfer is explained by the solution–diffusion model, proposed by Lonsdale et al. [7,8] and the preferential sorption–capillary flow model, proposed by Sourirajan et al. [8,9]. The main subject of investigation in the outside-membrane mass transfer is the mass transfer process near the membrane, where concentration–polarization (CP) significantly affects the mass transfer process. Hence, the study of outside-membrane mass transfer focuses on the modeling of CP; it is necessary to model the CP phenomenon to predict the RO separation process.

Various attempts were made to understand and describe the CP phenomenon by a theoretical analysis, and the main models were based on film theory, such as the Kimura–Sourirajan model [10–14] and the Spiegler–Kedem model [15–19], which are both related to the mass transfer coefficient. In other literature, a model based on the solution–diffusion mass transport theory, CP, and pressure-dependent dynamic membrane resistance was developed to predict the performance of RO for mixed salt and dye solutions [20,21]. Pastagia et al. [22] developed an unsteady-state mass transfer model for a binary solute system composed of reactive black dye and a reactive red dye. Moreover, Jamal [23] developed a model without CP for the prediction of feed concentration, permeate concentration, rejection, and flux as a function of the operating time. Overall, these models proved to be useful and applicable in the RO separation process.

The objective of this work was to research the mass transfer during the RO concentration process. To fulfill this requirement, a mathematical model based on glucose–water separation through an RO membrane was developed. Considering the actual structure of the RO membrane, the irreversible thermodynamic Spiegler–Kedem model is appropriate for describing the inside-membrane mass transfer, while a CP model based on the one-dimensional flow assumption was selected to explain the outside-membrane mass transfer. The mathematical model proposed in this study couples the CP model with the irreversible thermodynamic Spiegler–Kedem model. Experimental data (glucose concentration experiment) were obtained from the treatment of a pretreated glucose solution using a laboratory-scale RO system, and studies on the validation of the model using experimental results are presented The calculated results are consistent with the experimental data. Also, the expression of k is deduced.

2. Theory

In the RO separation process, the mass transfer occurs mainly in the feed boundary layer (CP layer) and inside the membrane. The general process of mass transfer is shown schematically in Figure 1. In order to build a mass transfer model, a one-dimensional flow is assumed to be valid for the transport of solvent and solute through the membrane. In addition, the CP layer is assumed to be fully developed. On this basis, the mass transfer equation is expressed as

$$J_w \cdot C_p = J_w \cdot C - D\frac{dc}{dx} \tag{1}$$

where J_w is the solvent (pure water) flux, C_p is the permeate solution concentration, C is the solute concentration in the C_P layer, and D is the diffusion coefficient. The Equation (1) is transformed into the following equation

$$D\frac{dc}{dx} = J_w \cdot C - J_w \cdot C_p \tag{2}$$

According to Figure 1, x ranges from 0 to δ_{cp}, and C ranges from C_f to $C_{\delta,1}$. Integrating Equation (2) gives the following equation

$$\frac{C_{\delta,1} - C_p}{C_f - C_p} = e^{\left(\frac{J_w \cdot \delta_{cp}}{D}\right)} = e^{\left(\frac{J_w}{k}\right)} \tag{3}$$

where $C_{\delta,1}$ is the solute concentration at the membrane surface (feed side, as shown in Figure 1), C_f is the feed solution concentration, δ_{cp} is the CP layer thickness, and k is the mass transfer coefficient in the CP layer and is defined as

$$k = \frac{D}{\delta_{cp}} \tag{4}$$

According to Figure 1, the solute flux J_s is expressed by the following equation

$$J_s = B_s(C_{\delta,1} - C_{\delta,2}) = B_s\left(C_{\delta,1} - C_p\right) = J_w \cdot C_p \tag{5}$$

where B_s is the solute transport coefficient.

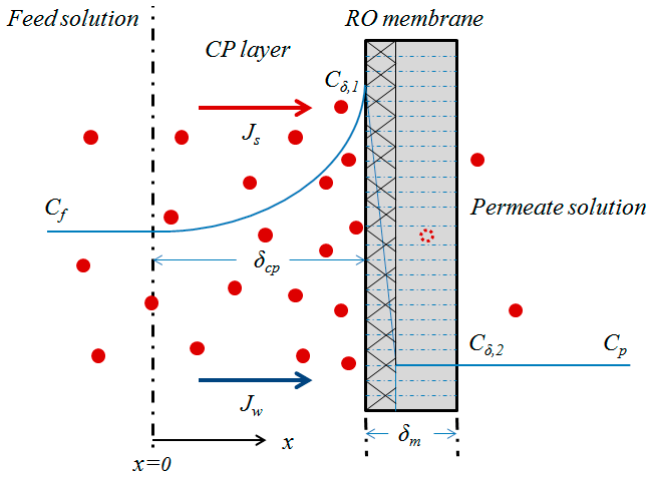

Figure 1. Schematic diagram of mass transfer in the reverse osmosis (RO) membrane separation process. CP: concentration–polarization.

For the reverse osmosis process, the total flux of the solvent and solute (J_v), which represents the volumetric flux on the permeate side of the RO membrane and can reflect the concentration capacity of the RO membrane, is expressed by the following equation

$$J_v = J_w + J_s \approx J_w \tag{6}$$

According to the principle of mass conservation, we get the following equations

$$Q_f C_f = Q_b C_b + Q_p C_p \tag{7}$$

$$Q_f = Q_b + Q_p \tag{8}$$

where Q_f, $Q_{b,}$, and Q_p are the feed solution flow, retentate flow, and permeate flow, respectively. C_b is the retentate solution concentration, and the relationship between Q_p and J_w is shown in the following equation

$$J_v = \frac{Q_p}{S} \tag{9}$$

where S is the effective RO membrane area.

The recovery (y), which represents the water production capacity, is defined as the fraction of the feed flow which passes through the membrane. The higher the recovery, the stronger the water production capacity of the RO system, and the stronger the concentration capacity of the RO system. The value of y is calculated by the following equation

$$y = \frac{Q_p}{Q_f} \times 100\% \tag{10}$$

To describe the mass transfer process of the RO membrane, we examined the parameters of the glucose solution and the microstructure of the RO membrane (PA2-4040, HYDECANME, HYDRANAUTICS, Oceanside, CA, USA). The effective thickness (calculated by deducting the thickness of the support layer) of the RO membrane was 0.2 μm. In contrast, the diameter of the glucose molecule ($<1 \times 10^{-3}$ μm) and the diameter of the water molecule ($\approx 4 \times 10^{-4}$ μm) are much smaller than the RO membrane thickness, and the membrane pore of the RO membrane was generally less than 1 nm (roughly the same as the diameter of the glucose molecule). Therefore, we believe that the solution interacted with the RO membrane during the membrane separation of the glucose solution, and the solution-diffusion model was discarded. In this work, the irreversible thermodynamic Spiegler–Kedem

model [24–27] was assumed to be appropriate for explaining the separation performance of solute through the membrane. Therefore, J_v is expressed by the following equation

$$J_v = L_p(\Delta p - \sigma\Delta\pi) \tag{11}$$

where L_p is the hydraulic permeability constant, $\triangle p$ is the transmembrane pressure, $\triangle\pi$ is the difference in the osmotic pressure across the membrane, and σ is the reflection coefficient. The reflection coefficient represents the solute separation capability of a membrane, where $\sigma = 0$ means no separation, and $\sigma = 1$ means complete separation (100% separation). For permeable membranes, $0 < \sigma < 1$. $\triangle\pi$ is calculated using the following equation

$$\Delta\pi = RT(C_{\delta,1} - C_{\delta,2}) = RT\left(C_{\delta,1} - C_p\right) \tag{12}$$

where R is the gas law constant, T is the temperature, and $C_{\delta,2}$ is the solute concentration at the membrane surface (permeate side, as shown in Figure 1).

The observed membrane rejection fraction R_o is given by

$$R_o = \frac{C_f - C_p}{C_f} \tag{13}$$

and the real rejection fraction R_r is given by

$$R_r = \frac{C_{\delta,1} - C_{\delta,2}}{C_{\delta,1}} = \frac{C_{\delta,1} - C_p}{C_{\delta,1}} \tag{14}$$

According to the Spiegler–Kedem equation, the real rejection fraction R_r is expressed as

$$R_r = \frac{\sigma(1-F)}{1-\sigma F} \tag{15}$$

F is defined as

$$F = \exp[-J_v(1-\sigma)/B_s] \tag{16}$$

where B_s is the solute transport coefficient.

Rewriting Equation (15), we get

$$J_v = \frac{B_s}{1-\sigma} \ln \frac{\sigma(1-R_r)}{\sigma - R_r} \tag{17}$$

Substituting Equations (13) and (14) in Equation (3), we get

$$\ln\left(\frac{1-R_o}{R_o}\right) = \frac{J_v}{k} + \ln\left(\frac{1-R_r}{R_r}\right) \tag{18}$$

Rewriting Equation (18), we get

$$k = J_v / \ln \frac{R_r(1-R_o)}{R_o(1-R_r)} \tag{19}$$

Substituting Equations (3) and (12) in Equation (11), we get

$$J_v = L_p(\Delta p - \sigma\Delta\pi) = L_p\left[\Delta p - \sigma RT\left(C_f - C_p\right)e^{\left(\frac{J_v}{k}\right)}\right] \tag{20}$$

Substituting Equation (19) in Equation (20), we get

$$J_v = L_p\left[\Delta p - \sigma RT\left(C_f - C_p\right)\frac{R_r(1-R_o)}{R_o(1-R_r)}\right] \quad (21)$$

3. Experimental

3.1. Membrane and Module

A polyamide composite membrane (PA2-4040, HYDECANME, USA) was chosen as the reverse osmosis experiment membrane material in the present work. The membrane characteristics are shown in Table 1.

Table 1. Main characteristics of the used membrane.

Type	PA2-4040	
Membrane properties	Composition	polyamide
	Permeable capacity (average, $m^3 \cdot d^{-1}$)	7.2
	Effective membrane area (m^2)	7.9
	Recovery rate (single, %)	15
Usage conditions	Maximum pressure (Mpa)	4.14
	Temperature (°C)	5–45
	Maximum flow ($m^3 \cdot h^{-1}$)	3.6

The experimental device (Figure 2) mainly consisted of a cooling and heating circulation tank to change the temperature of the model solution, a pump for feeding the glucose solution, a valve (check valve) to control the solution flux, the reverse osmosis membrane module (including pressure gauges and a flow meter), and a device for sampling the solution.

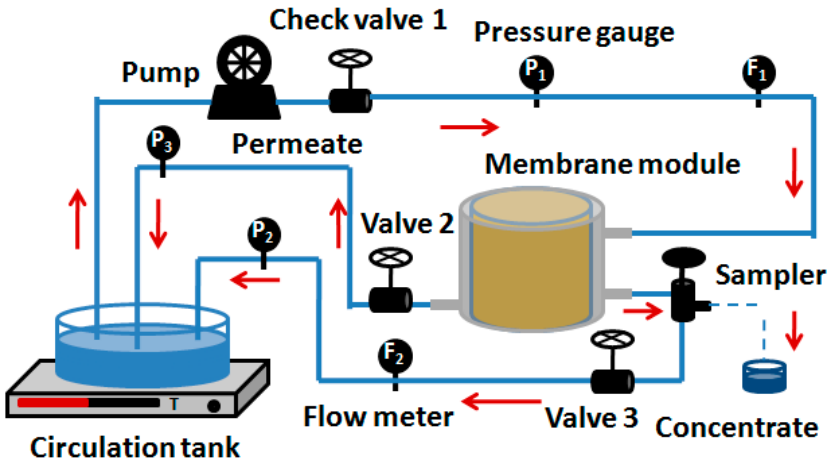

Figure 2. Schematic illustration of the reverse osmosis system.

3.2. Preparation of Model Solutions and Concentration Experiment

In this study, glucose anhydrous (AR) was purchased from the Kelong Chemical Reagent Factory, Chengdu, China. Model solutions (24.8–166.8 $mol \cdot m^{-3}$) were prepared using ultrapure water, by adding suitable amounts of the analytes (calculated).

The glucose model solutions were selected to carry out reverse osmosis concentration experiments using the reverse osmosis system (Figure 2). Model solutions were transferred into the membrane module by a feed pump. This was followed by the outflow of concentrate and permeate from the reverse osmosis membrane module and the reflow into the circulation tank. During this procedure, the concentrate was sampled by a sampling device and subsequently analyzed to evaluate the separation

effect of the reverse osmosis system. The concentrations of the glucose solutions (amount of sample for each test: 20 μL) were quantified using a high-performance liquid chromatography system (HPLC, Agilent LC1200, Agilent, Santa Clara, CA, USA) equipped with a differential refraction detector (RID) and an Aminex HPX-87H column (Bio-Rad Co., Hercules, CA, USA). Experimental data were measured three times to obtain an average value under each experimental condition.

4. Results and Discussion

4.1. Influence of Experimental Parameters of the Reverse Osmosis System

The pump used was a vertical multistage centrifugal pump (CDLF1, 50HZ, CNP, Hangzhou, China), and in the experimental design, one of the valves was installed at the outlet of the RO membrane (valve 3, Figure 2). The feed flow and transmembrane pressure in the system were changed by adjusting the valve 3. The relationship between the feed solution and transmembrane pressure is shown in Figure 3. According to Figure 3, the feed flow rate decreased when the transmembrane pressure increased, and the two parameters were roughly linear.

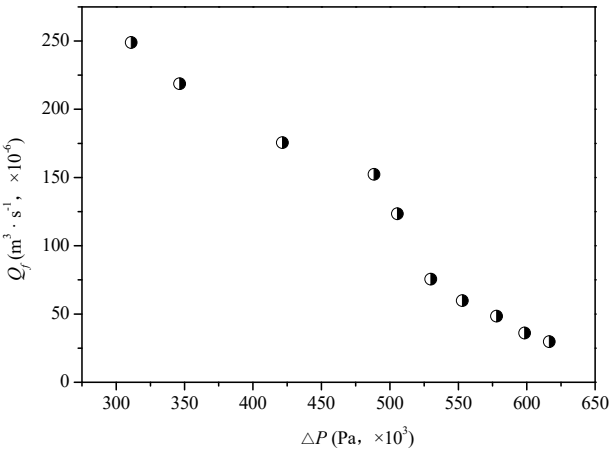

Figure 3. Relation between the feed solution flow and the transmembrane pressure.

Figure 4 reflects the effect of transmembrane pressure on the RO process. According to Figure 4, within the range of experimental parameters (310 kPa < $\triangle p$ < 617 kPa; 36 mol·m^{-3} < C_f < 140 mol·m^{-3}), when other experimental conditions are constant, J_v, y, R_o, and C_b increase with an increase in transmembrane pressure. J_v and $\triangle p$ are approximately linear, which is consistent with the irreversible thermodynamic Spiegler–Kedem model selected in this paper (Equation (11)). As the $\triangle p$ increased, y increased slowly, followed by an increase in growth rate, and the C_b maintained approximately the same trend. According to Equation (10), the recovery formula is a ratio. Combined with Figure 3 and J_v trend over $\triangle p$. In the formula of y, the numerator increases linearly with $\triangle p$ (consistent with the trend of J_v, Equation (9)), and the denominator decreases approximately linearly with $\triangle p$. Therefore, the overall ratio should increase, and the rate of the value increase should be gradual, which is consistent with the trend of y in Figure 4. According to Figure 4b, with the increase of $\triangle p$, R_o is slightly improved, although the trend is not obvious. According to Figure 3, Q_f decreased with increases of $\triangle p$. This means that a unit volume of feed solution can acquire more pressure to facilitate the RO process. The macroscopic performance of this process was an increase in R_o and J_v.

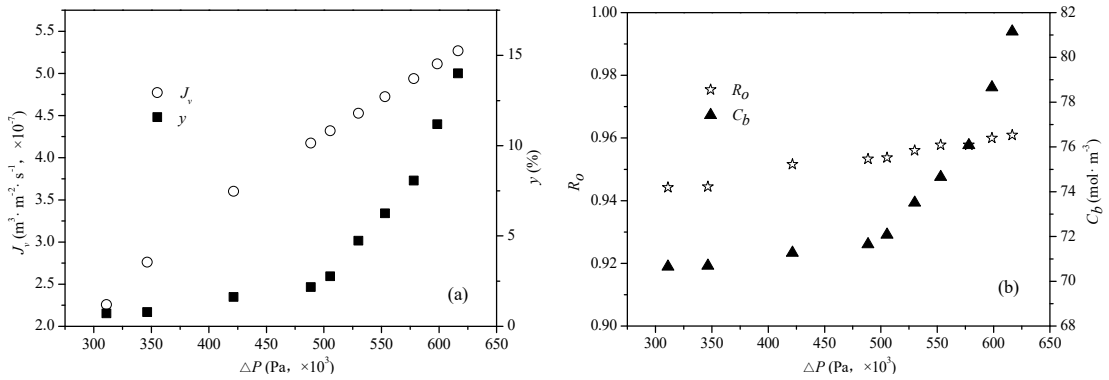

Figure 4. Influence of transmembrane pressure on RO process. (**a**) Solvent flux and recovery vary with transmembrane pressure, feed solution concentrate (C_f) = 70.17 mol·m^{-3}, pH = 6, T = 306 K; (**b**) Solute rejection and retentate solution concentration vary with transmembrane pressure, feed solution concentrate (C_f) = 70.17 mol·m^{-3}, pH = 6, T = 306 K.

Figure 5 shows the effect of C_f on the RO process. It can be seen in Figure 5 that an increase in C_f led to an increase in the C_b and decreases in J_v and y. The trend of R_o was not significant (slightly lower trend). In the RO process, the CP phenomenon occurs near the boundary layer of the membrane. When Q_f is constant, the increase in C_f leads to an enhanced CP phenomenon, which can result in a decrease in J_v, followed by a decrease in y. On the other hand, the enhancement of the CP phenomenon also leads to a slightly lower trend for R_o. The trend of C_b increasing with C_f was predictable and imaginable.

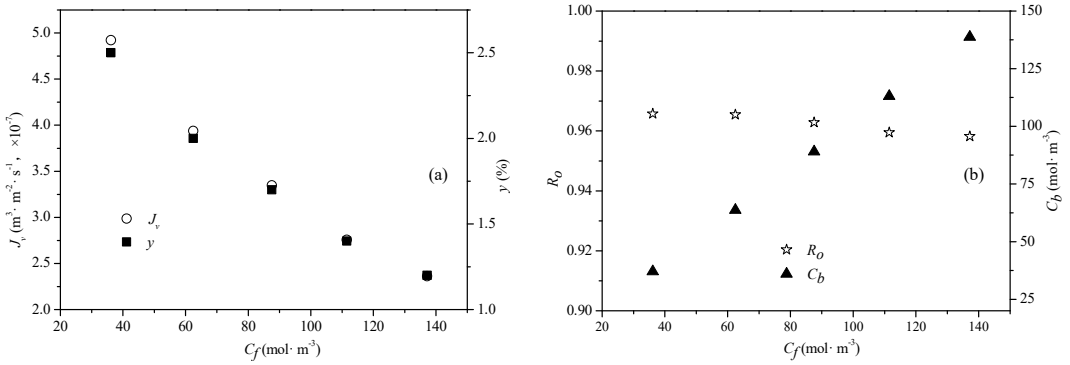

Figure 5. Influence of the feed solution concentration on RO process. (**a**) Solvent flux and recovery vary with feed solution concentration, feed solution flow (Q_f) = 1.56 × 10^{-4} m^3·s^{-1}, pH = 6, T = 306 K; (**b**) Solute rejection and retentate solution concentration vary with feed solution concentration, feed solution flow (Q_f) = 1.56 × 10^{-4} m^3·s^{-1}, pH = 6, T = 306 K.

4.2. Model Validation

Some mathematical formulas for the mass transfer in the RO process were given in the previous section (Section 2). In this section, model validation was carried out to verify that the calculated values of these mathematical formulas were consistent with the experimental data. In order to verify the models, we first determined some parameter values in the model. The non-linear parameter estimation technique of Levenberg–Marquardt, combined with the Gauss–Newton algorithm [17,20,28–31], was used in this study to estimate the parameters, and the calculated values of Bs and σ were 0.85 × 10^{-8} m·s^{-1} and 0.9981, respectively. We also calculated the Lp and $C_{\delta,1}$; the results are shown in Table 2. From Table 2 and Equation (14), we further calculated the real rejection fraction R_r. As shown in Table 2, Lp remained basically the same.

Table 2. Solute concentration at the membrane surface (C_f = 70.17 mol·m^{-3}, pH = 6, T = 306 K, R = 8.314 J·mol^{-1}·K^{-1}).

Q_f (m^3·s^{-1}, ×10^{-6})	$\triangle p$ (Pa, ×10^3)	C_p (mol·m^{-3})	$C_{\delta,1}$ (mol·m^{-3})	Lp (m·s^{-1}·Pa^{-1}, ×10^{-12})
248.8889	311	3.9142	70.57104	1.3923
218.6111	346.5	3.8976	70.72304	1.3611
175.5556	421.5	3.3972	71.06723	1.3423
152.2222	488.5	3.2748	71.49108	1.3238
123.3333	505.5	3.2471	71.97543	1.3048
75.5556	530	3.0858	73.44194	1.3889
59.7222	553	2.9635	74.33926	1.3709
48.3333	578	2.9635	75.48901	1.3538
36.1111	598.5	2.8078	77.80078	1.353
29.7222	616.5	2.7411	79.9817	1.3529

In the RO experiment, the feed solution flow Q_f and the permeate flow Q_p were obtained according to the flow meter. Then, the solvent (pure water) flux J_v was obtained (experimental value) based on Equation (9). Combined with Equation (21) and Table 2, we calculated the J_v (theoretical value). The comparison of the two J_v values is shown in Figure 6. Meanwhile, we calculated the relative error between each group of two J_v values, and the maximum value of the relative error was 12.81%.

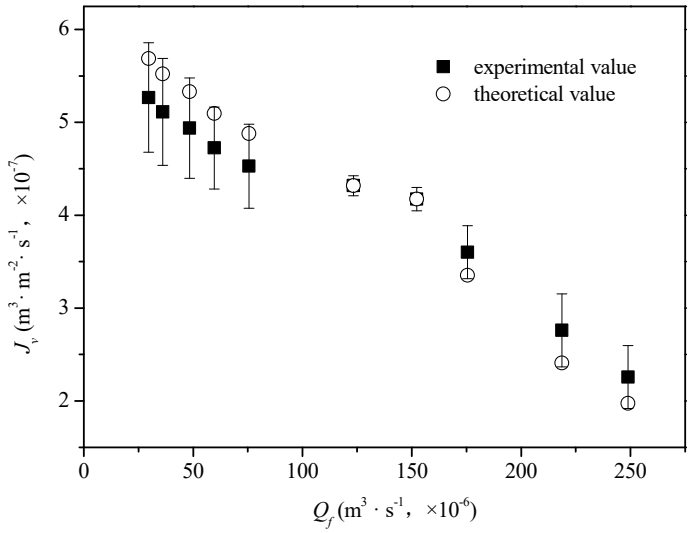

Figure 6. Comparison of the experimental and theoretical solvent flux values.

4.3. Estimation of the Mass Transfer Coefficient, k

The mass transfer coefficient (k) represents the transfer rate of the solute in the CP layer. The k value can reflect the strength of the concentration polarization, and with a known k value, the salt diffusion coefficient and boundary layer thickness can be determined using a dimensionless analysis. The RO membrane (PA2-4040, HYDECANME, USA) used in this work was a spiral wound membrane. The mass transfer coefficient (k) was calculated according to the following empirical formula [12]

$$k = \alpha Re^{\beta} Sc^{\gamma} \frac{D}{d_h} \tag{22}$$

where α, β, and γ are constants that vary for different physical situations, which are determined experimentally, and Re is the Reynolds number. Experiments indicate that the flow rate of the fluid, the fluid channel size, and the physical properties of the fluid (density and viscosity) affect the type of flow. These main influencing factors can be combined into a dimensionless parameter (Re), the value

of which can reflect the type of flow. *Sc* is the Schmidt number, and d_h is the hydraulic diameter of the channel. *Re* and *Sc* are defined as

$$Re = \frac{\rho u d_h}{\mu}, Sc = \frac{\mu}{\rho D} \tag{23}$$

where u, ρ, and μ are the velocity, the density, and the viscosity of the fluid, respectively.

For a spiral wound membrane, d_h is approximated by the following formula

$$d_h \approx 2h \tag{24}$$

where h is the rectangular feed channel thickness (h = 0.7112 mm, HYDECANME).

According to Equation (22) and the experimental work of this article, When Q_f changes during the RO process (since the C_f does not change, *Sc* and D/d_h are constant) only *Re* changes. Therefore, Equation (22) is rewritten by the following equation

$$k = \alpha_1 Re^{\beta} \tag{25}$$

where α_1 represents a combination constant.

Combining Table 2 with Equation (19), we can calculate the value of *k* and *Re* under different feed solution flow conditions (as shown in Table 3), then we performed a power function fitting according to Table 3 and Equation (25) and β = 0.9243. Equation (22) is rewritten by the following equation

$$k = \alpha Re^{0.9243} Sc^{\gamma} \frac{D}{d_h} \tag{26}$$

Table 3. Value of the mass transfer coefficient (*k*) and Reynolds number (*Re*) under different Q_f (C_f = 70.17 mol·m^{-3}, pH = 6, T = 306 K, R = 8.314 J·mol^{-1}·K^{-1}).

Q_f (m^3·s^{-1}, ×10^{-6})	k (m·s^{-1}, ×10^{-6})	d_h (m, ×10^{-4})	*Re*	*Sc*
248.8889	37.6	1.4224	151.2	482
218.6111	33.61	1.4224	132.8	482
175.5556	27.15	1.4224	106.6	482
152.2222	21.33	1.4224	92.5	482
123.3333	16.29	1.4224	74.9	482
75.5556	9.49	1.4224	45.9	482
59.7222	7.86	1.4224	36.3	482
48.3333	6.49	1.4224	29.4	482
36.1111	4.77	1.4224	21.9	482
29.7222	3.88	1.4224	18.1	482

Also, when C_f changed during the RO process, ρ, μ, and D of the solution were slightly changed as a result of the change in the concentration of the solution, leading to a slight change in *Re*. Since the change in *Re* was slight, we ignored it ($Re \approx 95$) in this paper. Equation (22) is rewritten by the following equation

$$k = \alpha_2 Sc^{\gamma} \tag{27}$$

where α_2 represents a variable value.

We calculated the value of *k* and *Sc* under different feed solution concentration conditions, as shown in Table 4, and the value of D was estimated from the literature [30]). According to Table 4, using the same method as above, the value of γ was obtained (γ = 0.3495). Equation (22) was rewritten by the following equation

$$k = \alpha Re^{0.9243} Sc^{0.3495} \frac{D}{d_h} \tag{28}$$

Table 4. Value of k and Schmidt number (Sc) under different C_f (Q_f = 155.56 × 10^{-6} $m^3 \cdot s^{-1}$, pH = 6, T = 306 K, R = 8.314 $J \cdot mol^{-1} \cdot K^{-1}$).

C_f (mol·m^{-3})	k (m·s^{-1}, ×10^{-6})	Sc	D/d_h (m·s^{-1}, ×10^{-6})
36.1567	22.2	484	1.1710
62.4444	21.95	482	1.1703
87.5533	21.77	480	1.1696
111.506	21.6	479	1.1689
137.149	21.4	478	1.1682

Finally, we calculated the value of α according to Table 4 and modified the value of α according to Table 3, α = 0.031, and obtained the final expression of the mass transfer coefficient

$$k = 0.031 Re^{0.9243} Sc^{0.3495} \frac{D}{d_h} \quad (29)$$

In this paper, according to Equation (29), the Reynolds number was the main factor affecting the mass transfer coefficient. Combining Table 3 and Equation (29), we plotted the experimental and theoretical values of k, as shown in Figure 7. We also calculated the relative error between each group of the two k values; the maximum value of the relative error was 12.2%.

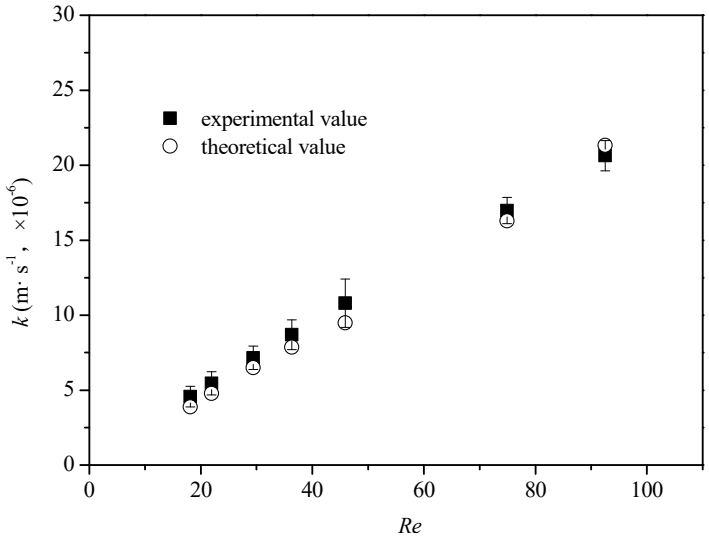

Figure 7. Comparison of the k values.

5. Conclusions

A mathematical modeling of glucose–water separation through an RO membrane was developed in this article. The model coupled the CP model, which used a one-dimensional flow assumption, with the irreversible thermodynamic Spiegler–Kedem model. The non-linear parameter estimation technique was used to determine the model parameters, such as L_p, σ, and B_s. Research on the validation of the model with experimental results was presented, and experimental data were obtained from the treatment of a pre-treated glucose solution using a laboratory-scale RO system. The comparison of the results showed that the calculated values were consistent with the experimental data. According to the calculated results, the maximum relative error between the two values was 12.81%. The expression of k was also deduced. The model well-describes the membrane performance during the mass transfer process, and the verification showed that the expression of k well-describes the reverse osmosis mass transfer of glucose solution.

Author Contributions: The concentrations of the glucose solutions were quantified by co-author H.Q. using HPLC, and the rest was completed independently by C.C.

Funding: This research was funded by Central Public-interest Scientific Institution Basal Research Fund [No. 12018206030202210_04]. And the APC was funded by Central Public-interest Scientific Institution Basal Research Fund [12016206030201701].

Acknowledgments: The authors are grateful to the Central Public-interest Scientific Institution Basal Research Fund [No. 12018206030202210_04] and Central Public-interest Scientific Institution Basal Research Fund [12016206030201701].

Conflicts of Interest: The authors declare no conflict of interest.

References

1. Atab, M.S.; Smallbone, A.J.; Roskilly, A.P. A hybrid reverse osmosis/adsorption desalination plant for irrigation and drinking water. *Desalination* **2018**, *444*, 44–52. [CrossRef]
2. Chung, T.S.; Zhang, S.; Wang, K.Y.; Su, J.; Ling, M.M. Forward osmosis processes: Yesterday, today and tomorrow. *Desalination* **2012**, *287*, 78–81. [CrossRef]
3. Ray, S.S.; Chen, S.S.; Sangeetha, D.; Chang, H.M.; Thanh, C.N.D.; Le, Q.H.; Ku, H.M. Developments in forward osmosis and membrane distillation for desalination of waters. *Environ. Chem. Lett.* **2018**, *16*, 1247–1265. [CrossRef]
4. Ray, S.S.; Chen, S.S.; Nguyen, N.C.; Nguyen, H.T.; Dan, N.P.; Thanh, B.X. Exploration of polyelectrolyte incorporated with Triton-X 114 surfactant based osmotic agent for forward osmosis desalination. *J. Environ. Manag.* **2018**, *209*, 346–353. [CrossRef] [PubMed]
5. Zhou, F.; Wang, C.; Wei, J. Separation of acetic acid from monosaccharides by NF and RO membranes: Performance comparison. *J. Membr. Sci.* **2013**, *429*, 243–251. [CrossRef]
6. Sundaramoorthy, S.; Srinivasan, G.; Murthy, D.V.R. An analytical model for spiral wound reverse osmosis membrane modules: Part I—Model development and parameter estimation. *Desalination* **2011**, *280*, 403–411. [CrossRef]
7. Lonsdale, H.K.; Merten, U.; Riley, R.L. Transport properties of cellulose acetate osmotic membranes. *J. Appl. Polym. Sci.* **1965**, *9*, 1341–1362. [CrossRef]
8. Merdaw, A.A.; Sharif, A.O.; Derwish, G.A.W. Water permeability in polymeric membranes, Part II. *Desalination* **2010**, *257*, 184–194. [CrossRef]
9. Soltanieh, M.; GILL', W.N. Review of reverse osmosis membranes and transport models. *Chem. Eng. Commun.* **1981**, *12*, 279–363. [CrossRef]
10. Goosen, M.F.A.; Sablani, S.; Cin, M.D.; Wilf, M. Effect of cyclic changes in temperature and pressure on permeation properties of composite polyamide seawater reverse osmosis membranes. *Sep. Sci. Technol.* **2010**, *46*, 14–26. [CrossRef]
11. Ghernaout, D. Reverse osmosis process membranes modeling—A historical overview. *J. Civ. Constr. Environ. Eng. Civ.* **2017**, *2*, 112–122.
12. Qiu, T.Y.; Davies, P.A. Concentration polarization model of spiral-wound membrane modules with application to batch-mode RO desalination of brackish water. *Desalination* **2015**, *368*, 36–47. [CrossRef]
13. Kim, D.Y.; Lee, M.H.; Gu, B.; Kim, J.H.; Lee, S.; Yang, D.R. Modeling of solute transport in multi-component solution for reverse osmosis membranes. *Desalin. Water Treat.* **2010**, *15*, 20–28. [CrossRef]
14. Khanarmuei, M.; Ahmadisedigh, H.; Ebrahimi, I.; Gosselin, L.; Mokhtari, H. Comparative design of plug and recirculation RO systems; thermoeconomic: Case study. *Energy* **2017**, *121*, 205–219. [CrossRef]
15. Spiegler, K.S.; Kedem, O. Thermodynamics of hyperfiltration (reverse osmosis): Criteria for efficient membranes. *Desalination* **1966**, *1*, 311–326. [CrossRef]
16. Jain, S.; Gupta, S.K. Analysis of modified surface force pore flow model with concentration polarization and comparison with Spiegler–Kedem model in reverse osmosis systems. *J. Membr. Sci.* **2004**, *232*, 45–62. [CrossRef]
17. Murthy, Z.V.P.; Chaudhari, L.B. Separation of binary heavy metals from aqueous solutions by nanofiltration and characterization of the membrane using Spiegler–Kedem model. *Chem. Eng. J.* **2009**, *150*, 181–187. [CrossRef]
18. Attarde, D.; Jain, M.; Gupta, S.K. Modeling of a forward osmosis and a pressure-retarded osmosis spiral wound module using the Spiegler-Kedem model and experimental validation. *Sep. Purif. Technol.* **2016**, *164*, 182–197. [CrossRef]

19. Hidalgo, A.M.; León, G.; Gómez, M.; Murcia, M.D.; Gómez, E.; Gómez, J.L. Application of the Spiegler–Kedem–Kachalsky model to the removal of 4-chlorophenol by different nanofiltration membranes. *Desalination* **2013**, *315*, 70–75. [CrossRef]
20. Ahmad, A.L.; Chong, M.F.; Bhatia, S. Mathematical modeling of multiple solutes system for reverse osmosis process in palm oil mill effluent (POME) treatment. *Chem. Eng. J.* **2007**, *132*, 183–193. [CrossRef]
21. Al-Bastaki, N. Removal of methyl orange dye and Na_2SO_4 salt from synthetic waste water using reverse osmosis. *Chem. Eng. Process. Process Intensif.* **2004**, *43*, 1561–1567. [CrossRef]
22. Pastagia, K.M.; Chakraborty, S.; DasGupta, S.; Basu, J.K.; De, S. Prediction of permeate flux and concentration of two-component dye mixture in batch nanofiltration. *J. Membr. Sci.* **2003**, *218*, 195–210. [CrossRef]
23. Jamal, K.; Khan, M.A.; Kamil, M. Mathematical modeling of reverse osmosis systems. *Desalination* **2004**, *160*, 29–42. [CrossRef]
24. Ślęzak, A. Irreversible thermodynamic model equations of the transport across a horizontally mounted membrane. *Biophys. Chem.* **1989**, *34*, 91–102. [CrossRef]
25. Van Gauwbergen, D.; Baeyens, J. Modelling reverse osmosis by irreversible thermodynamics. *Sep. Purif. Technol.* **1998**, *13*, 117–128. [CrossRef]
26. Sablani, S.S.; Goosen, M.F.A.; Al-Belushi, R.; Wilf, M. Concentration polarization in ultrafiltration and reverse osmosis: A critical review. *Desalination* **2001**, *141*, 269–289. [CrossRef]
27. Gupta, V.K.; Hwang, S.T.; Krantz, W.B.; Greenberg, A.R. Characterization of nanofiltration and reverse osmosis membrane performance for aqueous salt solutions using irreversible thermodynamics. *Desalination* **2007**, *208*, 1–18. [CrossRef]
28. Marquardt, D.W. An algorithm for least-squares estimation of nonlinear parameters. *J. Soc. Ind. Appl. Math.* **1963**, *11*, 431–441. [CrossRef]
29. Mendes, P.; Kell, D. Non-linear optimization of biochemical pathways: Applications to metabolic engineering and parameter estimation. *Bioinformatics* **1998**, *14*, 869–883. [CrossRef]
30. Dong, J.; Lu, K.; Xue, J.; Dai, S.; Zhai, R.; Pan, W. Accelerated nonrigid image registration using improved Levenberg–Marquardt method. *Inf. Sci.* **2018**, *423*, 66–79. [CrossRef]
31. Zhao, C.; Ma, P.; Zhu, C.; Chen, M. Measurement and correlation on diffusion coefficients of aqueous glucose solutions. *J. Chem. Ind. Eng.* **2005**, *56*, 1–5.